Quantum reading under a local energy constraint

Gaetana Spedalieri,[1,*] Cosmo Lupo,[2] Stefano Mancini,[2] Samuel L. Braunstein,[1] and Stefano Pirandola[1]
[1]*Department of Computer Science, University of York, York YO10 5GH, United Kingdom*
[2]*School of Science and Technology, University of Camerino, Camerino 62032, Italy*
(Received 16 April 2012; revised manuscript received 4 June 2012; published 13 July 2012)

Nonclassical states of light play a central role in many quantum information protocols. Very recently, their quantum features have been exploited to improve the readout of information from digital memories, modeled as arrays of microscopic beam splitters [Pirandola, Phys. Rev. Lett. **106**, 090504 (2011)]. In this model of "quantum reading," a nonclassical source of light with Einstein-Podolski-Rosen correlations has been proven to retrieve more information than any classical source. In particular, the quantum-classical comparison has been performed under a global energy constraint, i.e., by fixing the mean total number of photons irradiated over each memory cell. In this paper we provide an alternative analysis which is based on a local energy constraint, meaning that we fix the mean number of photons *per signal mode* irradiated over the memory cell. Under this assumption, we investigate the critical number of signal modes after which a nonclassical source of light is able to beat any classical source irradiating the same number of signals.

DOI: 10.1103/PhysRevA.86.012315 PACS number(s): 03.67.−a

I. INTRODUCTION

Quantum information has disclosed a modern approach to both quantum mechanics and information theory [1]. Very recently, this field has been further developed into the so-called "continuous-variable" domain, where information is encoded and processed by using quantum systems with infinite-dimensional Hilbert spaces [2–5] (see also the recent review [6]). The most important examples of these systems are the bosonic modes of the electromagnetic field, today manipulated with very high precision in quantum optics labs. Thus, within the continuous-variable framework, a wide range of results have been successfully achieved, including protocols of quantum teleportation [7–12], teleportation networks [13–17], entanglement swapping [18–20], quantum cryptography [21–30], quantum computation [31–39], and cluster quantum computation [40–45].

One of the key resources in quantum information is quantum entanglement. In the bosonic setting, quantum entanglement is usually present under the form of Einstein-Podolski-Rosen (EPR) correlations [46], where the quadrature operators of two separate bosonic modes are so correlated to beat the standard quantum limit [47]. The simplest source of EPR correlations is the two-mode squeezed vacuum (TMSV) state. In the number-ket representation, this state is defined by

$$|\xi\rangle = (\cosh\xi)^{-1}\sum_{n=0}^{\infty}(\tanh\xi)^n|n\rangle_s|n\rangle_i, \tag{1}$$

where ξ is the squeezing parameter and $\{s,i\}$ is an arbitrary pair of bosonic modes, that we may call "signal" and "idler."In particular, ξ quantifies the signal-idler entanglement and determines the mean number of photons $\sinh^2\xi$ in each mode. Since it is entangled, the TMSV state cannot be prepared by applying local operations and classical communications (LOCCs) to a couple of vacua $|0\rangle_s\otimes|0\rangle_i$ or to any other kind of tensor product state. For this reason, the TMSV state cannot be expressed as a classical mixture of coherent states $|\alpha\rangle_s\otimes|\beta\rangle_i$ with α and β arbitrary complex amplitudes. In other words, its $\mathcal{P}$ representation [48,49],

$$|\xi\rangle\langle\xi| = \iint d^2\alpha d^2\beta\mathcal{P}(\alpha,\beta)|\alpha\rangle_s\langle\alpha|\otimes|\beta\rangle_i\langle\beta|, \tag{2}$$

involves a function $\mathcal{P}$ which is nonpositive and, therefore, cannot be considered as a genuine probability distribution. For this reason, the TMSV state is a particular kind of "nonclassical" state. Other kinds are single-mode squeezed states and Fock states. By contrast, a bosonic state is called "classical" when its $\mathcal{P}$ representation is positive, meaning that the state can be written as a classical mixture of coherent states. Thus a classical source of light is composed by a set of m bosonic modes in a state

$$\rho = \int d^2\alpha_1\cdots\int d^2\alpha_m\mathcal{P}(\alpha_1,\ldots,\alpha_m)\otimes_{k=1}^m|\alpha_k\rangle\langle\alpha_k|, \tag{3}$$

where $\mathcal{P}$ is positive and normalized to 1. Typically, classical sources are made by just a collection of coherent states with amplitudes $\{\bar\alpha_1,\ldots,\bar\alpha_m\}$, i.e., $\rho=\otimes_{k=1}^m|\bar\alpha_k\rangle\langle\bar\alpha_k|$, which corresponds to having

$$\mathcal{P} = \prod_{k=1}^m\delta^2(\alpha_k-\bar\alpha_k). \tag{4}$$

In other situations, where the sources are particularly chaotic, they are better described by a collection of thermal states with mean photon numbers $\{\bar n_1,\ldots,\bar n_m\}$, so that

$$\mathcal{P} = \prod_{k=1}^m\frac{\exp(-|\alpha_k|^2\bar n_k)}{\pi\bar n_k}. \tag{5}$$

More generally, we can have classical states which are not just tensor products but they have (classical) correlations among different bosonic modes.

The comparison between classical and nonclassical states has clearly triggered a lot of interest. The main idea is to compare the use of a candidate nonclassical state, like the EPR state, with all the classical states for specific information tasks. One of these tasks is the detection of low-reflectivity objects

*gae.spedalieri@york.ac.uk

in far target regions under the condition of extremely low signal-to-noise ratios. This scenario has been called "quantum illumination" and has been investigated in a series of papers [50–55].

More recently, EPR correlations have been exploited for a completely different task in a completely different regime of parameters. In the model of "quantum reading" [56], EPR correlations have been used to retrieve information from digital memories which are reminiscent of today's optical disks, such as CDs and DVDs. A digital memory can in fact be modeled as a sequence of cells corresponding to beam splitters with two possible reflectivities, r_0 and r_1 (used to encode a bit of information). By fixing the mean total number of photons N irradiated over each memory cell, it is possible to show that a nonclassical source of light with EPR correlations retrieves more information than any classical source [56]. In general, the improvement is found in the regime of few photons ($N = 1$–100) and for memories with high reflectivities, as typical for optical memories. In this regime, the gain of information given by quantum reading can be dramatic, i.e., close to 1 bit for each bit of the memory. Further studies on quantum reading of memories have been pursued by several authors [57–63]. In particular, Ref. [57] shows that other nonclassical states, such as Fock states, can have remarkable advantages over classical sources. Reference [58] presents an alternative model of quantum reading based on a binary phase encoding. Reference [59] further studies the problem of binary discrimination in optical devices. Reference [60] both proposes and experimentally implements a model of unambiguous quantum reading. Reference [61] defines the notion of quantum reading capacity, a quantity which has been also investigated in Ref. [62]. Finally, Ref. [63] has proposed explicit capacity-achieving receivers for quantum reading.

It is fundamental to remark that an important point in the study of Ref. [56] is that the quantum-classical comparison is performed under a *global energy constraint*, i.e., by fixing the total average number of photons N which are irradiated over each memory cell [see Fig. 1(a)]. Under this assumption, it is possible to construct an EPR transmitter, made by a suitable number of TMSV states, which is able to outperform *any* classical source composed by *any* number of modes.

In this paper we consider a different kind of comparison: we fix the number of signal modes irradiated over the target cell (M) and the mean number of photons *per signal mode* (N_S). Under these assumptions, we compare an EPR transmitter with a classical source. Then, for fixed N_S, we determine the critical number of signal modes $M^{(N_S)}$ after which an EPR transmitter with $M > M^{(N_S)}$ is able to beat any classical source (with the same number of signals M). Since we are here fixing the average number of photons per signal mode, our energy constraint is now *local*: it restricts the energy of each signal mode but not the energy of the total set of signal modes. We call this alternative model "locally constrained quantum reading" [see Fig. 1(b)].

The difference between global and local energy constraints is also discussed in Ref. [6] for the general problem of Gaussian channel discrimination. Mathematically speaking, both these energy constraints make the problem of channel discrimination nontrivial in the continuous-variable setting, where the use of infinite energy always allows one to distinguish two Gaussian

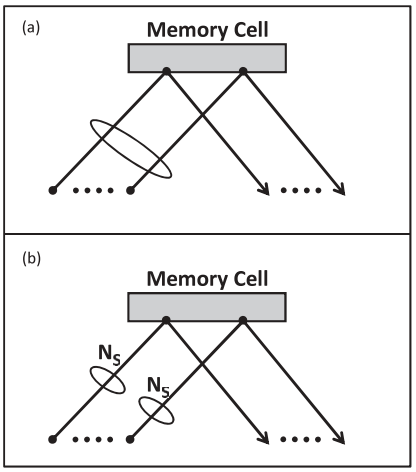

FIG. 1. Inset (a): Quantum reading of Ref. [56] is formulated under a global energy constraint. This means that we fix the total average number of photons N irradiated over the memory cell. Thus, if the number of input signals is M, each one has an average of N/M photons, which goes to zero for $M \to \infty$. Inset (b): In this paper, we consider an alternative model of quantum reading under a local energy constraint (locally constrained quantum reading). In this case, we fix the average number of photons N_S for each input signal. Since the total number of signals M can be arbitrary, we have that the total energy irradiated over the cell MN_S is generally unbounded.

channels in a perfect way. In the presence of a global energy constraint, the error probability in the Gaussian channel discrimination is generally different from zero and the problem is to find the minimum value. In the presence of a local energy constraint, the error probability goes to zero with the number M of signals and the general problem is to study its convergence, i.e., finding the best error exponent [6]. From this point of view, the present paper shows that the best convergence of the error probability has to be found within the set of nonclassical states.

From a practical point of view, the use of a local energy constraint is useful in all those situations where the energy of each radiation mode has to be taken under control. For instance, consider a photosensitive organic memory where data is encoded in error-correcting blocks. For simplicity, we may think of blocks of M cells where information is encoded by means of an M-bit repetition code (the generalization to more complex codes such as the Reed-Solomon codes is only a technical issue [64]). In this scenario, the stored information can be safely retrieved from the block if we irradiate a single mode per cell with suitable low energy (for instance, a single temporal mode, i.e., a pulse, with a mean energy N_S which is below the critical energy associated with the photodegradation of the material). By contrast, optimizing the readout under a global energy constraint may be unsafe in this specific situation, since the optimal readout of the block could be achieved by concentrating all the available energy into a single mode. Thus, if we use a total of $N = MN_S$ mean photons, we could have all these photons irradiated over a single cell of the block, with inevitable damage for the memory.

The remainder of the paper is structured as follows. In Sec. II we review the basic readout mechanism of quantum reading specifying the analysis to the case of a local energy

constraint. Then, in Sec. III we explicitly show how EPR correlations can be used to beat any classical source of light in the readout of information. Finally, Sec. IV is for conclusions. Note that we also provide two appendices. In Appendix A we discuss the general mathematical methods used in our derivations, and Appendix B contains some technical proofs.

II. READOUT MECHANISM

Here we briefly review the basic readout mechanism of Ref. [56], specifying the study to the case of a local energy constraint. Consider a model of a digital optical memory (or disk) where the memory cells are beam-splitter mirrors with different reflectivities $r = r_0, r_1$ (with $r_1 \geqslant r_0$). In particular, the bit value $u = 0$ is encoded in a lower-reflectivity mirror ($r = r_0$), that we may call a *pit*, while the bit value $u = 1$ is encoded in a higher-reflectivity mirror ($r = r_1$), that we may call a *land* (see Fig. 2). Close to the disk, a reader aims to retrieve the value of the bit u which is stored in each memory cell. For this purpose, the reader exploits a transmitter (to probe a target cell) and a receiver (to measure the corresponding output). In general, the transmitter consists of two quantum systems, called *signal* S and *idler* I, respectively. The signal system S is a set of M bosonic modes which are directly shined on the target cell. The mean total number of photons of this system is simply given by $N = MN_S$, where N_S is the mean number of photons per signal mode (simply called "energy," hereafter). At the output of the cell, the reflected system R is combined with the idler system I, which is a supplementary set of bosonic modes whose number L can be completely arbitrary. Both the systems R and I are finally measured by the receiver (see Fig. 2).

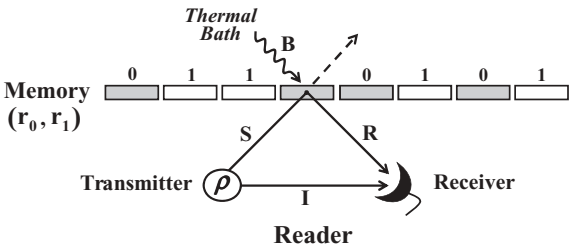

FIG. 2. **Model of memory**. Digital information is stored in a disk whose memory cells are beam-splitter mirrors with different reflectivities: $r = r_0$ encoding bit value $u = 0$, and $r = r_1$ encoding bit value $u = 1$. **Readout**. A reader is generally composed of a transmitter and a receiver. It retrieves a stored bit by probing a memory cell with a signal system S (composed of M bosonic modes) and detecting the reflected system R together with an idler system I (composed of L bosonic modes). In general, the output system R combines the signal system S with a bath system B (M bosonic modes in thermal states). The transmitter is in a state ρ which can be classical (a classical transmitter) or nonclassical (a quantum transmitter). In particular, we consider a quantum transmitter with EPR correlations between the signal and idler systems. In this paper, the quantum-classical comparison is performed under a local energy constraint, i.e., by fixing the average number of photons N_S per signal mode. (The signal system S has a total average number of photons $N = MN_S$, which is generally unbounded.)

We assume that Alice's apparatus is very close to the disk, so that no significant source of noise is present in the gap between the disk and the decoder. However, we assume that non-negligible noise comes from the thermal bath present at the other side of the disk. This bath generally describes stray photons, transmitted by previous cells and bouncing back to hit the next ones. For this reason, the reflected system R combines the signal system S with a bath system B of M modes. These environmental modes are assumed in a tensor product of thermal states, each one with N_B mean photons (white thermal noise). Thus, in this model we identify five basic parameters: the reflectivities of the memory $\{r_0, r_1\}$, the temperature of the bath N_B, and the profile of the signal $\{M, N_S\}$, which is given by the number of signals M and the energy N_S.

In general, for a fixed input state ρ at the transmitter (systems S, I), Alice will get two possible output states σ_0 and σ_1 at the receiver (systems R, I). These output states are the effect of two different quantum channels, $\mathcal{E}_0$ and $\mathcal{E}_1$, which depend on the bit $u = 0, 1$ stored in the target cell. In particular, we have

$$\sigma_u = (\mathcal{E}_u \otimes \mathcal{I})(\rho), \tag{6}$$

where the conditional channel $\mathcal{E}_u$ acts on the signal system, while the identity channel $\mathcal{I}$ acts on the idler system. More precisely, we have $\mathcal{E}_u = \mathcal{R}_u^{\otimes M}$, where $\mathcal{R}_u$ is a one-mode lossy channel with conditional loss r_u and fixed thermal noise N_B. Now, the minimum error probability P_{err} affecting the decoding of u is just the error probability affecting the statistical discrimination of the two output states, σ_0 and σ_1, via an optimal receiver. This quantity is equal to

$$P_{\text{err}} = [1 - D(\sigma_0, \sigma_1)]/2, \tag{7}$$

where $D(\sigma_0, \sigma_1)$ is the trace distance between σ_0 and σ_1 [65–67]. Clearly, the value of P_{err} determines the average amount of information which is decoded for each bit stored in the memory. This quantity is equal to

$$J = 1 - H(P_{\text{err}}), \tag{8}$$

where

$$H(x) := -x \log_2 x - (1 - x) \log_2 (1 - x) \tag{9}$$

is the usual formula for the binary Shannon entropy. In the following, we compare the performance of decoding in two paradigmatic situations, one where the transmitter is described by a nonclassical state (a quantum transmitter) and one where the transmitter is in a classical state (a classical transmitter). In particular, we show how a quantum transmitter with EPR correlations (an EPR transmitter) is able to outperform classical transmitters. The quantum-classical comparison is performed for a fixed signal profile $\{M, N_S\}$. Then, for various fixed values of the energy N_S (local energy constraint), we study the critical number of signal modes $M^{(N_S)}$ after which an EPR transmitter (with $M > M^{(N_S)}$ signals) is able to beat any classical transmitter (with the same number of signals M).

III. QUANTUM-CLASSICAL COMPARISON

First let us consider a classical transmitter. A classical transmitter with M signals and L idlers is described by a classical state ρ as specified by Eq. (3) with $m = M + L$. In

other words, it is a probabilistic mixture of multimode coherent states $\otimes_{k=1}^{M+L}|\alpha_k\rangle\langle\alpha_k|$. Given this transmitter, we consider the corresponding error probability $P_{\rm err}^{\rm class}$ which affects the readout of the memory. Remarkably, this error probability is lower bounded by a quantity which depends on the signal profile $\{M,N_S\}$, but not from the number L of the idlers and the explicit expression of the $\mathcal{P}$ function. In fact, we have [56]

$$P_{\rm err}^{\rm class} \geqslant \mathcal{C}(M,N_S) := \frac{1-\sqrt{1-F(N_S)^M}}{2}, \tag{10}$$

where $F(N_S)$ is the fidelity between $\mathcal{R}_0(|N_S^{1/2}\rangle\langle N_S^{1/2}|)$ and $\mathcal{R}_1(|N_S^{1/2}\rangle\langle N_S^{1/2}|)$, the two possible outputs of the single-mode coherent state $|N_S^{1/2}\rangle\langle N_S^{1/2}|$ (see Appendix A for more details). As a consequence, all the classical transmitters with signal profile $\{M,N_S\}$ retrieve information which is upper bounded by

$$J_{\rm class} := 1 - H[\mathcal{C}(M,N_S)]. \tag{11}$$

Now, let us construct a transmitter having the same signal profile $\{M,N_S\}$ but possessing EPR correlations between signals and idlers. This is realized by taking M identical copies of a TMSV state, i.e., $\rho = |\xi\rangle\langle\xi|^{\otimes M}$, where $N_S = \sinh^2\xi$. Given this transmitter, we consider the corresponding error probability $P_{\rm err}^{\rm quant}$ affecting the readout of the memory. This quantity is upper bounded by the quantum Chernoff bound [68–72]

$$P_{\rm err}^{\rm quant} \leqslant \mathcal{Q}(M,N_S) := \tfrac{1}{2}[Q(N_S)]^M, \tag{12}$$

where

$$Q(N_S) := \inf_{s\in(0,1)} {\rm Tr}\left(\theta_0^s\theta_1^{1-s}\right) \tag{13}$$

and

$$\theta_u := (\mathcal{R}_u\otimes\mathcal{I})(|\xi\rangle\langle\xi|). \tag{14}$$

Since θ_0 and θ_1 are Gaussian states, we can write out their symplectic decompositions [73] and compute the quantum Chernoff bound using the formula for multimode Gaussian states given in Ref. [72] (see Appendix A for more details). Then, we can easily compute a lower bound,

$$J_{\rm quant} := 1 - H[\mathcal{Q}(M,N_S)], \tag{15}$$

for the information which is decoded via this quantum transmitter.

In order to show an improvement with respect to the classical case, it is sufficient to prove the positivity of the "information gain:"

$$G := J_{\rm quant} - J_{\rm class}. \tag{16}$$

This quantity is in fact a lower bound for the average information, which is gained by using the EPR quantum transmitter over any classical transmitter. Roughly speaking, the value of G estimates the minimum information which is gained by the quantum readout for each bit of the memory. In general, G is a function of all the basic parameters of the model, i.e., $G = G(M,N_S,r_0,r_1,N_B)$. Numerically, we can easily find signal profiles $\{M,N_S\}$, classical memories $\{r_0,r_1\}$, and thermal baths N_B, for which we have the quantum effect $G > 0$. Some of these values are reported in Table I.

TABLE I. Information gain G for various choices of the basic parameters.

M	N_S	r_0	r_1	N_B	G(bits)
1	3.5	0.5	0.95	0.01	6.2×10^{-3}
10	1	0.2	0.8	0.01	3.4×10^{-2}
30	1	0.38	0.85	1	1.2×10^{-3}
100	0.1	0.25	0.85	0.01	5.9×10^{-2}
200	0.1	0.6	0.95	0.01	0.22
2×10^5	0.01	0.995	1	0	0.99

Note that we can find choices of parameters where $G \simeq 1$, i.e., the classical readout of the memory does not decode any information whereas the quantum readout is able to retrieve all of it. As shown in the last row of the table, this situation can occur when both the reflectivities of the memory are very close to 1. From the first row of the table, we can observe another remarkable fact: for a land reflectivity r_1 sufficiently close to 1, one signal with a few photons can give a positive gain. In other words, the use of a single, but sufficiently entangled, TMSV state $|\xi\rangle\langle\xi|$ can outperform any classical transmitter, which uses one signal mode with the same energy (and potentially infinite idler modes).

Here an important point to remark is that, once that we find a positive gain $G > 0$, this positivity is preserved if we increase the number of signals M. In other words, if G is positive for some $\tilde{M}$, then it is positive for every $M \geqslant \tilde{M}$ (keeping the other parameters fixed). This is trivial to prove. In fact, $G(\tilde{M}) > 0$ is equivalent to $\mathcal{Q}(\tilde{M},N_S) < \mathcal{C}(\tilde{M},N_S)$, which is equivalent to

$$\frac{1}{2}Q^{\tilde{M}} < \frac{1-\sqrt{1-F^{\tilde{M}}}}{2}, \tag{17}$$

according to Eqs. (10) and (12). This means that

$$Q < (1-\sqrt{1-F^{\tilde{M}}})^{1/\tilde{M}}. \tag{18}$$

For every $M \geqslant \tilde{M}$, we then have

$$Q^M < (1-\sqrt{1-x})^m, \tag{19}$$

where $m := M/\tilde{M}$ and $x := F^{\tilde{M}}$. Now we can use the algebraic inequality

$$(1-\sqrt{1-x})^m \leqslant 1-\sqrt{1-x^m}, \tag{20}$$

which holds for every $m \geqslant 1$ and $x \in [0,1]$. We then get

$$Q^M < 1-\sqrt{1-F^M}, \tag{21}$$

which is equivalent to

$$\mathcal{Q}(M,N_S) < \mathcal{C}(M,N_S) \tag{22}$$

for every $M \geqslant \tilde{M}$.

Thanks to this property, for given reflectivities $\{r_0,r_1\}$ and bath temperature N_B, i.e., for a fixed memory, if a quantum transmitter with signal profile $\{\tilde{M},N_S\}$ outperforms the classical transmitters, then any other quantum transmitter with the same energy N_S and $M \geqslant \tilde{M}$ is also able to beat the classical readout.

It is also important to note that the advantage of quantum transmitters over classical transmitters is asymptotically negligible in the limit of a large number of signals. Mathematically

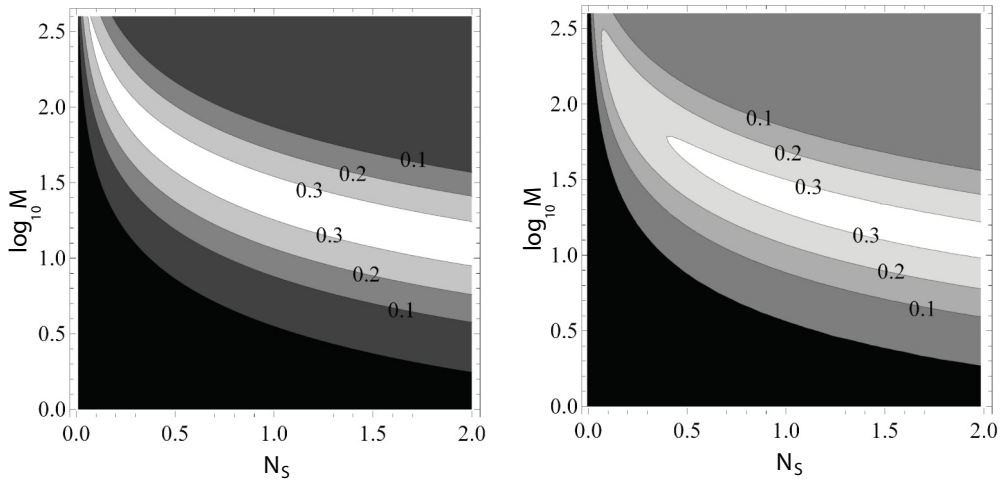

FIG. 3. Contour plots of the information gain G^* as a function of the signal energy N_S and the number of signal modes M (in logarithmic scale). Reflectivities are $r_0 = 0.6$ and $r_1 = 0.95$. Thermal noise is $N_B = 10^{-3}$ (left plot) and $N_B = 10^{-2}$ (right plot). In the bottom black area, we have $G^* = 0$. The maximum values of G^* are taken in the intermediate white area where $G^* \gtrsim 0.3$ bits. For a large number of modes M, we have $G^* \to 0$.

speaking, the information gain $G = G(M,N_S,r_0,r_1,N_B)$ always goes to zero for $M \to +\infty$. This is clearly a consequence of the specific constraint that we consider in this work, for which the limit of $M \to +\infty$ corresponds to the limit of infinite energy, a regime where any transmitter is able to retrieve information with negligible error probability. In fact, given a memory with two reflectivities $r_0 \neq r_1$ and finite temperature N_B, an arbitrary transmitter in any tensor product state $\rho = \omega^{\otimes M}$ has error probability

$$P_{\text{err}} \leqslant \frac{Q^M}{2}, \tag{23}$$

where the quantum Chernoff bound Q is evaluated over the single-copy output states. Now, for nonzero signal energy $N_S > 0$, we have $Q < 1$, so that $P_{\text{err}} \to 0$ for $M \to +\infty$. The situation is clearly different from Ref. [56], where the global energy constraint is adopted, i.e., the mean total number of photons N is fixed. In that case, the broadband limit $M \to +\infty$ implies a vanishing energy per signal mode $N_S = NM^{-1}$. As a result, we have $Q \to 1$ and the upper bound no longer guarantees that P_{err} tends to zero. As a matter of fact, in Ref. [56], the broadband limit is absolutely nontrivial and gives the optimal gain for the most important class of memories.

Contrary to what happens in Ref. [56], in the present model of locally constrained quantum reading we have that the maximum advantage, i.e., the optimal gain G, occurs for intermediate values of the signal mode number M. Given a memory with parameters $\{r_0,r_1,N_B\}$, there is an optimal range of numbers M depending on the signal energy of the transmitter N_S. In order to numerically investigate this behavior, we consider an estimate for the information gain $G^* \leqslant G$ which is provided by using the quantum Battacharyya bound in the place of the quantum Chernoff bound [72]. In other words, we consider

$$G^* := J^*_{\text{quant}} - J_{\text{class}}, \tag{24}$$

where

$$J^*_{\text{quant}} := 1 - H[\mathcal{B}(M,N_S)] \tag{25}$$

and

$$\mathcal{B}(M,N_S) := \tfrac{1}{2}\left[\text{Tr}\left(\theta_0^{1/2}\theta_1^{1/2}\right)\right]^M \tag{26}$$

is the quantum Battacharyya bound computed over the two equiprobable output states θ_0 and θ_1.

Given a memory specified by a set of parameters $\{r_0,r_1,N_B\}$, we can study the information gain G^* as a function of the signal profile $\{M,N_S\}$. This is done in Figs. 3–5. As we can see from Fig. 3, the information gain G^* is zero for low values of M (black area in the figure). It takes its maximum for M belonging to an intermediate range of values (this range corresponds to the white area in the figure). Then, for higher values of M, the value of G^* gradually decreases to zero. For a memory with reflectivities $r_0 = 0.6$ and $r_1 = 0.95$ and affected by a thermal noise $N_B = 10^{-3} - 10^{-2}$, we can reach an optimal gain $G^* \gtrsim 0.3$ by using around $M = 10$ modes with $N_S = 2$. At lower energies, we achieve the same performance by using more signal modes.

In Fig. 4 we consider a memory of better quality, i.e., with higher reflectivities (equal to $r_0 = 0.95$ and $r_1 = 0.98$, respectively). As we can see from the figure, the information gain can reach optimal values above 0.7 bits if we consider around $M = 10^3$ signals.

Finally, in Fig. 5 we consider even better memories, with high reflectivities and low thermal noise. As we can see from the figure, gains above 0.8 bits can be reached by using $M = 10^2 - 10^3$ signal modes.

A. Ideal memories

According to our numerical investigation, the quantum readout is generally more powerful when the land reflectivity is sufficiently high (i.e., $r_1 \gtrsim 0.8$). For this reason, it is very important to analyze the scenario in the limit of ideal land reflectivity ($r_1 = 1$). Using the terminology of Ref. [56], we

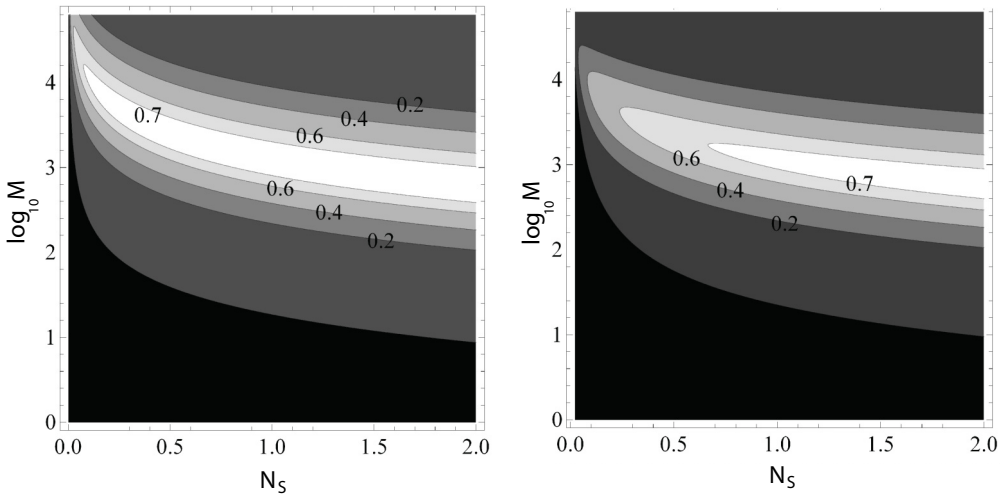

FIG. 4. Contour plots of the information gain G^* as a function of the signal energy N_S and the number of signal modes M (in logarithmic scale). Reflectivities are $r_0 = 0.95$ and $r_1 = 0.98$. Thermal noise is $N_B = 10^{-3}$ (left plot) and $N_B = 10^{-2}$ (right plot). In the bottom black area, we have $G^* = 0$. The maximum values of G^* are taken in the intermediate white area where $G^* \gtrsim 0.7$ bits. For a large number of modes M, we have $G^* \to 0$.

call an "ideal memory" a classical memory with $r_1 = 1$. Clearly, this memory is completely characterized by the value of its pit reflectivity r_0. For ideal memories, the quantum Chernoff bound of Eq. (12) takes an analytical form given by the "Chernoff term,"

$$Q(N_S) = \frac{1}{[1 + (1 - \sqrt{r_0})N_S]^2 + N_B(2N_S + 1)(1 - r_0)}, \tag{27}$$

and the classical bound of Eq. (10) can be computed using

$$F(N_S) = \gamma^{-1} \exp[-\gamma^{-1}(1 - \sqrt{r_0})^2 N_S], \tag{28}$$

where $\gamma := 1 + (1 - r_0)N_B$ (see Appendix A for more details). Using these formulas, we can study the behavior of the gain G in terms of the remaining parameters $\{M, N_S, r_0, N_B\}$.

Let us consider an ideal memory with generic $r_0 \in [0,1)$ in a generic thermal bath $N_B \geqslant 0$. For a fixed energy N_S, we consider the minimum number of signals $M^{(N_S)}$ above which $G > 0$. To be precise, the critical number $M^{(N_S)}$ that we consider is a solution of the equation $G = 0$. From this real value we derive the minimum number of signals (which is an integer) by taking its ceiling function $\lceil M^{(N_S)} \rceil$. The critical number $M^{(N_S)}$ can be defined independently from the thermal noise N_B by performing a numerical maximization over N_B. Then, for a given value of the energy N_S, the critical number $M^{(N_S)}$ becomes a function of r_0 alone, i.e., $M^{(N_S)} = M^{(N_S)}(r_0)$. Its behavior is shown in Fig. 6 for different values of the energy.

It is remarkable that for low-energy signals ($N_S = 0.01 - 1$ photons), the critical number $M^{(N_S)}(r_0)$ is finite for every $r_0 \in [0,1)$. This means that for ideal memories and low-energy

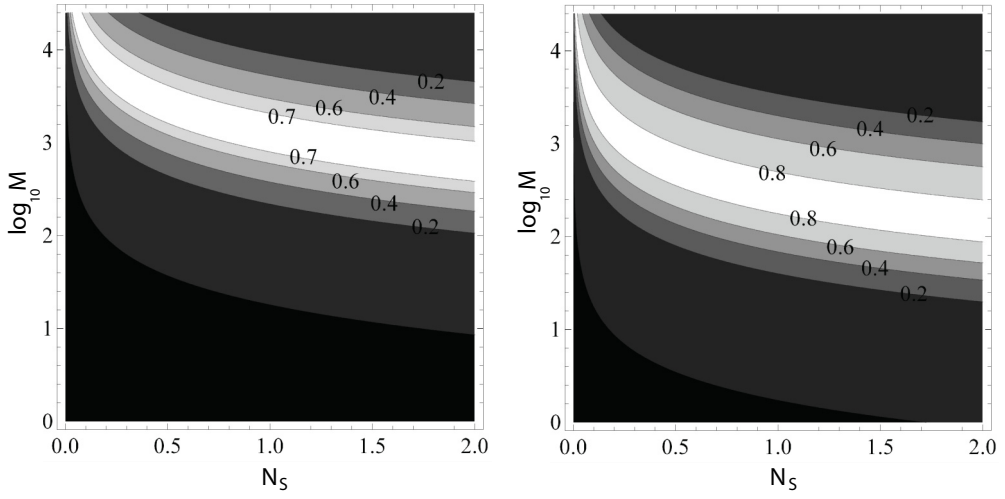

FIG. 5. Contour plots of the information gain G^* as a function of the signal energy N_S and the number of signal modes M (in logarithmic scale). Thermal noise is equal to $N_B = 10^{-5}$. In the left plot, reflectivities are $r_0 = 0.95$ and $r_1 = 0.98$. In the right plot, reflectivities are $r_0 = 0.95$ and $r_1 = 0.999$. In the bottom black area, we have $G^* = 0$. The maximum values of G^* are taken in the intermediate white area where $G^* \gtrsim 0.7$ (left) and $G^* \gtrsim 0.8$ (right). For large number of modes M, we have $G^* \to 0$.

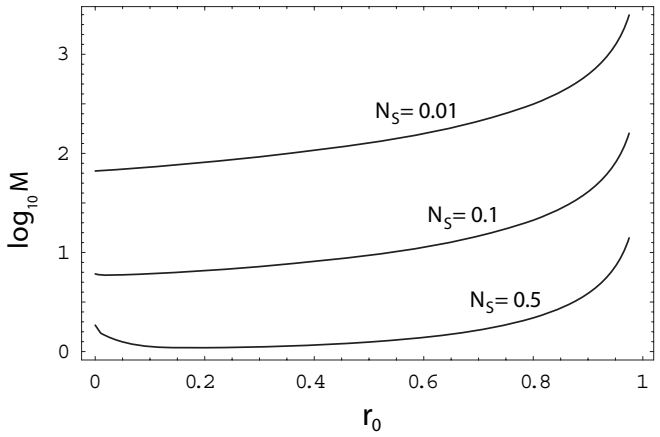

FIG. 6. Number of signals M (logarithmic scale) versus pit reflectivity r_0. The curves refer to $N_S = 0.01$, 0.1, and 0.5 photons. For each value of the energy N_S, we plot the critical number $M^{(N_S)}(r_0)$ as a function of r_0. All the curves have an asymptote at $r_0 = 1$. For $N_S \gtrsim 2.5$ photons (curves not shown), we have another asymptote at $r_0 = 0$.

signals, there always exists a finite number of signals $M^{(N_S)}$ above which the quantum readout of the memory is more efficient than its classical readout. In other words, there is an EPR transmitter with $M > M^{(N_S)}$ able to beat any classical transmitter with the same number of signals M. In the low-energy regime considered, $M^{(N_S)}(r_0)$ is relatively small for almost all the values of r_0, except for $r_0 \to 1$ where $M^{(N_S)}(r_0) \to \infty$. In fact, for $r_0 \simeq 1$, we derive

$$M^{(N_S)}(r_0) \simeq [4N_S(2N_S + 1)(1 - r_0)]^{-1}, \tag{29}$$

which diverges at $r_0 = 1$. Such a divergence is expected, since we must have $P_{\rm err}^{\rm quant} = P_{\rm err}^{\rm class} = 1/2$ for $r_0 = r_1$ (see Appendix B for details). Apart from the divergence at $r_0 = 1$, in all the other points $r_0 \in [0,1)$, the critical number $M^{(N_S)}(r_0)$ decreases for increasing energy N_S (see Fig. 6). In particular, for an $N_S = 1$ photon, we have $M^{(N_S)}(r_0) \simeq 1$ for most of the reflectivities r_0. In other words, for energies around one photon, a single TMSV state is sufficient to provide a positive gain for most of the ideal memories. However, the decreasing trend of $M^{(N_S)}(r_0)$ does not continue for higher energies ($N_S \geqslant 1$). In fact, just after $N_S = 1$, $M^{(N_S)}(r_0)$ starts to increase around $r_0 = 0$. In particular, for $N_S \geqslant 1$, we can derive

$$M^{(N_S)}(0) \simeq (\ln 2)[2\ln(1 + N_S) - N_S]^{-1}, \tag{30}$$

which is increasing in N_S and becomes infinite at $N_S \simeq 2.5$. As a consequence, for $N_S \gtrsim 2.5$ photons, we have a second asymptote appearing at $r_0 = 0$ (see Appendix B for more details). This means that the use of high-energy signals ($N_S \gtrsim 2.5$) does not assure positive gains for memories with extremal reflectivities $r_0 = 0$ and $r_1 = 1$.

IV. CONCLUSION

In conclusion, we have considered the basic model of digital memory studied in Ref. [56], which is composed of beam-splitter mirrors with different reflectivities. Adopting this model, we have compared an EPR transmitter with classical sources for fixed signal profiles, finding positive information gains for memories with high land reflectivities ($r_1 \gtrsim 0.8$). Analytical results can be derived in the limit of ideal land reflectivity ($r_1 = 1$), which defines the regime of ideal memories. In this case, by fixing the mean number of photons per signal mode (local energy constraint), we have computed the critical number of signals above which an EPR transmitter gives positive information gains, therefore beating any classical transmitter. For low-energy signals (0.01–1 photons) this critical number is finite and relatively small for every ideal memory. In particular, an EPR transmitter with one TMSV state can be sufficient to achieve positive information gains for almost all the ideal memories.

Thus our results corroborate the outcomes of Ref. [56], providing an alternative study which considers a local energy constraint instead of a global one. As discussed in Ref. [56] and its supplementary materials, potential applications are in the technology of optical digital memories where we could increase data-transfer rates and storage capacities. For instance, let us fix the mean signal power P which is irradiated on the memory cell during the readout time t. This is approximately given by $P = h\nu N t^{-1}$, where h is the Planck constant, ν is the carrier frequency, and N is mean total number of photons. Suppose that we can access low values of N_S using a reasonably low number of modes M so that the value of N is globally low. Now, at fixed power and frequency, the low-energy regime (low N) corresponds to short readout times t, i.e., high data-transfer rates. Equivalently, at fixed power and readout time, the low-energy regime corresponds to high frequencies ν, i.e., dense storage devices.

Finally, another potential application is the readout of organic digital memories, which are devices extremely photosensitive at high frequencies. In this case, the use of faint quantum signals could safely read the data without damaging the storing devices. As discussed before, locally constrained quantum reading may be particularly suitable for the readout of these fragile memories thanks to the direct control of the mean energy of each radiation mode.

APPENDIX A: METHODS

Here we provide more details about the methods used in our computations. We start with a brief review of the bosonic Gaussian states (Appendix A 1). Then we give a detailed description of the readout problem, discussing the main techniques for computing the performances of classical and nonclassical transmitters (Appendix A 2). Finally, we consider the special case of ideal memories, for which we can derive simple analytical formulas (Appendix A 3).

1. Bosonic systems and Gaussian states

A bosonic system is generally composed of n modes. This means that the system is associated with a tensor product Hilbert space $\mathcal{H}^{\otimes n}$ and described by a vector of quadrature operators

$$\hat{\mathbf{x}}^T := (\hat{q}_1, \hat{p}_1, \ldots, \hat{q}_n, \hat{p}_n), \tag{A1}$$

which satisfy the commutation relations $[\hat{x}_k,\hat{x}_l] = 2i\Omega_{kl}$, where

$$\mathbf{\Omega} := \bigoplus_{i=1}^{n} \begin{pmatrix} 0 & 1 \\ -1 & 0 \end{pmatrix} \tag{A2}$$

defines a symplectic form (correspondingly, a real matrix $\mathbf{S}$ is called "symplectic" if $\mathbf{S\Omega S}^T = \mathbf{\Omega}$).

By definition, a bosonic state ρ is "Gaussian" if its Wigner function is Gaussian [6]. As a result, a Gaussian state ρ is fully characterized by its first- and second-order statistical moments. These are the displacement vector

$$\bar{\mathbf{x}} := \mathrm{Tr}(\hat{\mathbf{x}}\rho) \tag{A3}$$

and the covariance matrix (CM) $\mathbf{V}$, with generic element

$$V_{kl} := \tfrac{1}{2}\mathrm{Tr}(\{\hat{x}_k,\hat{x}_l\}\rho) - \bar{x}_k\bar{x}_l, \tag{A4}$$

where $\{,\}$ is the anticommutator. The CM is a $2n \times 2n$ real symmetric matrix which must satisfy the uncertainty principle [6,74]

$$\mathbf{V} + i\mathbf{\Omega} \geqslant 0. \tag{A5}$$

According to Williamson's theorem [75], every CM $\mathbf{V}$ can be decomposed in the form

$$\mathbf{V} = \mathbf{SWS}^T, \tag{A6}$$

where $\mathbf{S}$ is a symplectic matrix and

$$\mathbf{W} = \bigoplus_{i=1}^{n} \nu_i \mathbf{I} = \begin{pmatrix} \nu_1 & & & & \\ & \nu_1 & & & \\ & & \ddots & & \\ & & & \nu_n & \\ & & & & \nu_n \end{pmatrix} \tag{A7}$$

is called the "Williamson form" of $\mathbf{V}$. In this matrix, the diagonal elements $\{\nu_1,\ldots,\nu_n\}$ represent the "symplectic spectrum" of $\mathbf{V}$. The symplectic spectrum provides powerful ways to express physical properties of the Gaussian state. For instance, the uncertainty principle can be formulated as [6,73]

$$\mathbf{V} > 0, \quad \nu_i \geqslant 1. \tag{A8}$$

2. Quantum reading versus classical reading

In our model of classical memory, each memory cell is represented by a beam-splitter mirror with two possible reflectivities, i.e., the pit reflectivity r_0 and the land reflectivity r_1. This dichotomic choice $r \in \{r_0,r_1\}$ is used to encode an information bit $u \in \{0,1\}$ in the memory cell. Then, one side of the memory is subject to decoding, while the other side is affected by white thermal noise, with average photon number per mode equal to N_B. It is clear that this model of memory corresponds to a problem of Gaussian channel discrimination. In fact, each memory cell can be seen as an attenuator channel, transforming an input-signal mode into an output-reflected mode. In particular, this attenuator channel has a transmission efficiency (or "linear loss") which is given by the dichotomic reflectivity of the cell $r \in \{r_0,r_1\}$ and a thermal noise which is fixed and equal to N_B. Depending on the bit $u \in \{0,1\}$ which is stored in the cell, we then have two possible attenuator channels that we denote $\mathcal{R}_0$ and $\mathcal{R}_1$. In other words, the unknown bit u stored in the cell is encoded into a conditional attenuator channel $\mathcal{R}_u$.

Let us describe explicitly the action of $\mathcal{R}_u$. Given the quadratures $\hat{\mathbf{x}}_s^T := (\hat{q}_s,\hat{p}_s)$ of an input signal mode s, the quadratures $\hat{\mathbf{x}}_r$ of the output-reflected mode r are given by the Heisenberg relation,

$$\hat{\mathbf{x}}_r = \sqrt{r}\hat{\mathbf{x}}_s + \sqrt{1-r}\hat{\mathbf{x}}_b, \tag{A9}$$

where $r \in \{r_0,r_1\}$ and $\hat{\mathbf{x}}_b$ are the quadratures of a bath mode b. In particular, the bath mode is described by a thermal state $\rho_b(N_B)$ with N_B average photons, i.e., a Gaussian state with zero mean and CM

$$\mathbf{V}_b = (2N_B + 1)\mathbf{I}. \tag{A10}$$

Once we have specified the action of a memory cell over an arbitrary signal mode s, we can analyze its full action on an arbitrary transmitter. In general, we have a system S of M signal modes impinging on the cell, besides an ancillary system I of L idler modes which bypass the cell. At the output of the cell, the system R of the M reflected modes is combined with the idler system I in a joint measurement at the receiver. The fundamental parameters of the transmitter are contained in its signal profile $\{M,N_S\}$, which is composed by the number of signal modes M and the average number of photons per signal N_S.

Let us denote by ρ_{SI} the global state of the input systems $\{S,I\}$. The memory cell does not affect the idler system I but acts on the signal system S by coupling every signal mode $s \in S$ with an independent thermal mode b, which belongs to a bath system B in the multimode thermal state

$$\rho_B = \rho_b(N_B)^{\otimes M}. \tag{A11}$$

Since the action on the signal system S is one-mode and conditional, the global state of the output systems $\{R,I\}$ can be written as

$$\rho_{RI}(u) = \left(\mathcal{R}_u^{\otimes M} \otimes \mathcal{I}^{\otimes L}\right)(\rho_{SI}), \tag{A12}$$

where $\mathcal{I}^{\otimes L}$ is the identity channel acting on the idler system. For a fixed state ρ_{SI} at the transmitter, we have a conditional output state $\rho_{RI}(u)$ at the receiver, which depends on the bit u stored in the memory cell. Thus, the minimum error probability in decoding the stored bit is just the error probability affecting the optimal discrimination of the two output states $\rho_{RI}(0)$ and $\rho_{RI}(1)$. As we know, this error probability is equal to [65]

$$P_{\mathrm{err}} = \tfrac{1}{2}\left\{1 - D[\rho_{RI}(0),\rho_{RI}(1)]\right\}, \tag{A13}$$

where $D[\rho_{RI}(0),\rho_{RI}(1)]$ is the trace distance between $\rho_{RI}(0)$ and $\rho_{RI}(1)$. Clearly, the value of P_{err} determines the average amount of information which is decoded for each bit stored in the memory. This average information is equal to $J = 1 - H(P_{\mathrm{err}})$, where $H(x)$ is the usual formula of the binary Shannon entropy.

In our work, we estimate the average decoded information J in two paradigmic situations, i.e., for a quantum transmitter with EPR correlations (J_Q), and for a generic classical transmitter (J_C). By fixing the signal profile $\{M,N_S\}$, we compare J_Q and J_C. More exactly, we fix all the basic

parameters of the model, i.e., besides fixing the signal profile $\{M,N_S\}$, we also fix the reflectivities of the memory $\{r_0,r_1\}$ and the thermal noise N_B. Then, we investigate what are the values of the basic parameters $\{M,N_S,r_0,r_1,N_B\}$ for which $J_Q > J_C$. In particular, for proving this enhancement, we compare a lower bound of J_Q with an upper bound of J_C.

a. Classical transmitters

Let us start considering an arbitrary classical transmitter. For a classical transmitter with M signals and L idlers, we can exploit the classical discrimination bound proven in Ref. [56]. The minimum error probability $P_{\rm err}^{\rm class}$ affecting the readout of the memory cell is lower bounded by $\mathcal{C}(M,N_S)$ in Eq. (10), where $F(N_S)$ is the fidelity between the two states $\mathcal{R}_0(|N_S^{1/2}\rangle\langle N_S^{1/2}|)$ and $\mathcal{R}_1(|N_S^{1/2}\rangle\langle N_S^{1/2}|)$. Using the formula of the fidelity for single-mode Gaussian states [77–79], we get

$$F(N_S) = \frac{1}{\sqrt{\gamma^2+\theta}-\sqrt{\theta}} \exp\left[-\frac{(\sqrt{r_1}-\sqrt{r_0})^2}{\gamma} N_S\right], \tag{A14}$$

where

$$\gamma = 1 + (2 - r_0 - r_1)N_B \tag{A15}$$

and

$$\theta = 4N_B^2 \prod_{i=0,1} (1-r_i)[1+(1-r_i)N_B]. \tag{A16}$$

Notice that the lower-bound $\mathcal{C}(M,N_S)$ depends on the signal profile $\{M,N_S\}$, but not from the number L of idlers and the explicit $\mathcal{P}$ representation describing the classical state of the transmitter. As a consequence, all the classical transmitters with the same signal profile $\{M,N_S\}$ are lower bounded by $\mathcal{C}(M,N_S)$. The average information J_C which is decoded from the memory cell is upper bounded by the quantity

$$J_{\rm class} := 1 - H[\mathcal{C}(M,N_S)]. \tag{A17}$$

b. Quantum transmitter

Now, let us consider a quantum transmitter with the same signal profile $\{M,N_S\}$ but possessing EPR correlations between signals and idlers (EPR quantum transmitter). In this case, we have the same number of signals and idlers ($M = L$), and the global state for the input systems $\{S,I\}$ is a tensor product of M identical two-mode squeezed vacuum states, i.e.,

$$\rho_{SI} = |\xi\rangle_{si}\langle\xi|^{\otimes M}, \tag{A18}$$

where the single-copy state $|\xi\rangle_{si}\langle\xi|$ refers to a single pair of signal and idler modes $\{s,i\} \in \{S,I\}$. Recall that a two-mode squeezed vacuum state $|\xi\rangle_{si}\langle\xi|$ is a Gaussian state with zero mean and CM

$$\mathbf{V}_{si} = \begin{pmatrix} (2N_S+1)\mathbf{I} & 2\sqrt{N_S(N_S+1)}\mathbf{Z} \\ 2\sqrt{N_S(N_S+1)}\mathbf{Z} & (2N_S+1)\mathbf{I} \end{pmatrix}, \tag{A19}$$

where $\mathbf{I} = \mathrm{diag}(1,1)$, $\mathbf{Z} = \mathrm{diag}(1,-1)$, and the squeezing parameter ξ is connected to the signal energy by the relation $N_S = \sinh^2\xi$. At the output of the cell, the conditional state of the systems $\{R,I\}$ is given by

$$\rho_{RI}(u) = \rho_{ri}(u)^{\otimes M}, \tag{A20}$$

where

$$\rho_{ri}(u) = (\mathcal{R}_u \otimes \mathcal{I})(|\xi\rangle_{si}\langle\xi|) \tag{A21}$$

is the single-copy output state, i.e., describing a single pair of reflected and idler modes $\{r,i\} \in \{R,I\}$. In fact, since the memory cell corresponds to a one-mode channel and the state of the transmitter to a tensor product, the output state at the receiver is also a tensor product state. In particular, it corresponds to M identical copies of the two-mode state of Eq. (A21). Then, the decoding of u corresponds to the M-copy discrimination between the two states $\rho_{ri}(0)$ and $\rho_{ri}(1)$. The corresponding minimum error probability $P_{\rm err}^{\rm quant}$ can be upper bounded by the quantum Chernoff bound, i.e.,

$$P_{\rm err}^{\rm quant} \leqslant \mathcal{Q}(M,N_S) := \tfrac{1}{2}[Q(N_S)]^M, \tag{A22}$$

where

$$Q(N_S) := \inf_{s\in(0,1)} \mathrm{Tr}[\rho_{ri}(0)^s \rho_{ri}(1)^{1-s}]. \tag{A23}$$

Notice that the single-copy state $\rho_{ri}(u)$ is a Gaussian state with zero mean and CM

$$\mathbf{V}_{ri}(u) = \begin{pmatrix} [r_u\mu + (1-r_u)\beta]\mathbf{I} & \sqrt{r_u(\mu^2-1)}\mathbf{Z} \\ \sqrt{r_u(\mu^2-1)}\mathbf{Z} & \mu\mathbf{I} \end{pmatrix}, \tag{A24}$$

where

$$\mu := 2N_S + 1, \quad \beta := 2N_B + 1. \tag{A25}$$

Since $\rho_{ri}(0)$ and $\rho_{ri}(1)$ are two-mode Gaussian states, we can compute the quantum Chernoff bound $\mathcal{Q}(M,N_S)$ by using the formula of Ref. [72], which exploits the symplectic decomposition of the Gaussian states. It is important to note that the CM of Eq. (A24) is in a special form, for which we can easily provide analytical expressions for both the symplectic spectrum and the diagonalizing symplectic matrix $\mathbf{S}$. In fact, let us set

$$a := r_u\mu + (1-r_u)\beta, \quad b := \mu \tag{A26}$$

and

$$c := \sqrt{r_u(\mu^2-1)} \geqslant 0, \tag{A27}$$

so that the CM takes the special normal form

$$\mathbf{V} = \begin{pmatrix} a\mathbf{I} & c\mathbf{Z} \\ c\mathbf{Z} & b\mathbf{I} \end{pmatrix}. \tag{A28}$$

The corresponding symplectic eigenvalues are given by [6]

$$\nu_1 = \tfrac{1}{2}(\sqrt{y} + a - b) \tag{A29}$$

and

$$\nu_2 = \tfrac{1}{2}(\sqrt{y} + b - a), \tag{A30}$$

where $y := (a+b)^2 - 4c^2 \geqslant 4$. Thus, the Williamson form of $\mathbf{V}$ is given by

$$\mathbf{W} = \nu_1 \mathbf{I} \oplus \nu_2 \mathbf{I} = \frac{1}{2} \begin{pmatrix} (\sqrt{y}+a-b)\mathbf{I} & \\ & (\sqrt{y}+b-a)\mathbf{I} \end{pmatrix}. \quad \text{(A31)}$$

The symplectic matrix $\mathbf{S}$ which realizes the symplectic decomposition $\mathbf{V} = \mathbf{S}\mathbf{W}\mathbf{S}^T$ is given by the formula [6]

$$\mathbf{S} = \begin{pmatrix} x_+ \mathbf{I} & x_- \mathbf{Z} \\ x_- \mathbf{Z} & x_+ \mathbf{I} \end{pmatrix}, \quad \text{(A32)}$$

where

$$x_\pm := \sqrt{\frac{a+b \pm \sqrt{y}}{2\sqrt{y}}} \geqslant 0. \quad \text{(A33)}$$

Now, by writing the symplectic diagonalization for the two possible cases $u = 0$ and $u = 1$, we have

$$\mathbf{V}_{ri}(u) = \mathbf{S}(u)[\nu_1(u)\mathbf{I} \oplus \nu_2(u)\mathbf{I}]\mathbf{S}(u)^T. \quad \text{(A34)}$$

Using this decomposition, we can compute the quantum Chernoff bound by means of the formula of Ref. [72]. Unfortunately, the analytical expression is cumbersome, but we can easily derive numerical values for every choice of the parameters.

It is clear that from the upper bound $P_{\text{err}}^{\text{quant}} \leqslant \mathcal{Q}(M, N_S)$, we can derive a lower bound for the average information J_Q which is decoded via this quantum transmitter. This lower bound is simply given by

$$J_{\text{quant}} := 1 - H[\mathcal{Q}(M, N_S)]. \quad \text{(A35)}$$

c. Comparison

In order to compare quantum and classical reading, we fix the basic parameters of the model $\{M, N_S, r_0, r_1, N_B\}$ and we consider the difference

$$G := J_{\text{quant}} - J_{\text{class}}, \quad \text{(A36)}$$

that we have called "information gain."It is trivial to check that

$$G \leqslant J_Q - J_C. \quad \text{(A37)}$$

In other words, G is a lower bound for the average information which is gained by using the EPR quantum transmitter instead of any classical transmitter. A positive gain ($G > 0$) is a sufficient condition for the superiority of the quantum reading ($J_Q > J_C$). In general, this quantity is a function of all the basic parameters of the model, i.e., $G = G(M, N_S, r_0, r_1, N_B)$. Numerically, we can find signal profiles $\{M, N_S\}$, classical memories $\{r_0, r_1\}$, and thermal baths N_B for which we have the quantum effect $G > 0$. Some of these values are shown by the table in the main text. As explained in the main text, we can also resort to the further lower bound $G^* \leqslant G$, which is defined by using the quantum Battacharyya bound instead of the quantum Chernoff bound. By exploiting G^*, we can plot Figs. 3–5.

3. Ideal memories

Quantum reading is generally more powerful when the land reflectivity is sufficiently high (i.e., $r_1 \gtrsim 0.8$). For this reason, it is important to analyze the scenario in the limit of ideal land reflectivity ($r_1 = 1$), defining the so-called "ideal memories."In the presence of an ideal memory, one of the two possible outputs of the cell is just the input state, i.e., we have

$$\rho_{RI}(1) = \rho_{SI}. \quad \text{(A38)}$$

Clearly, this fact leads to a simplification of the calculus. In the case of an EPR quantum transmitter, the input state is pure and given by Eq. (A18). As a consequence, we have

$$\rho_{RI}(1) = \rho_{ri}(1)^{\otimes M} = |\xi\rangle_{si} \langle\xi|^{\otimes M}, \quad \text{(A39)}$$

i.e., one of the two output states is pure. Thus the quantum Chernoff bound can be reduced to the computation of the quantum fidelity. In fact, we have [76]

$$\begin{aligned} Q(N_S) &:= \inf_{s\in(0,1)} \text{Tr}[\rho_{ri}(0)^s \rho_{ri}(1)^{1-s}] \\ &= \inf_{s\in(0,1)} \text{Tr}[\rho_{ri}(0)^s |\xi\rangle_{si} \langle\xi|^{1-s}] \\ &= \lim_{s\to 1^-} \text{Tr}[\rho_{ri}(0)^s |\xi\rangle_{si} \langle\xi|^{1-s}] \\ &= F[\rho_{ri}(0), |\xi\rangle_{si} \langle\xi|], \end{aligned} \quad \text{(A40)}$$

where the fidelity $F[\rho_{ri}(0), |\xi\rangle_{si}\langle\xi|]$ is between a mixed two-mode Gaussian state $\rho_{ri}(0)$ with CM given in Eq. (A24) and a pure two-mode Gaussian state $|\xi\rangle_{si}\langle\xi|$ with CM given in Eq. (A19). Then we can apply the formula of Ref. [76] for the quantum fidelity between multimode Gaussian states. We achieve

$$\begin{aligned} Q(N_S) &= F[\rho_{ri}(0), |\xi\rangle_{si}\langle\xi|] \\ &= \frac{1}{[1+(1-\sqrt{r_0})N_S]^2 + N_B(2N_S+1)(1-r_0)}, \end{aligned} \quad \text{(A41)}$$

which is the result given in the main text.

In the case of a classical transmitter, we just have to consider the lower bound of Eq. (10) where now we set $r_1 = 1$ in the expression of the fidelity given in Eq. (A14). One can easily check that the resulting fidelity takes the analytical form given in Eq. (28).

APPENDIX B: TECHNICAL PROOFS

Here, we explicitly prove the asymptotic expansions which have been presented in the main text and used for the analysis of the ideal memories.

1. General asymptote ($r_0 = 1$)

According to Fig. 6, the critical number $M^{(N_S)}(r_0)$ diverges for $r_0 \to 1$. Let us analyze the behavior of G around the singular point $r_0 = 1$ by setting $r_0 = 1 - \varepsilon$ and expanding G for $\varepsilon \to 0^+$. It is easy to check that, for every N_B, we have $G > 0$ if and only if

$$M > [4N_S(2N_S+1)\varepsilon]^{-1}. \quad \text{(B1)}$$

In particular, in the absence of thermal noise ($N_B = 0$), we have

$$G = \frac{MN_S(4MN_S-1)\varepsilon^2}{8\ln 2} + O(\varepsilon^3), \quad \text{(B2)}$$

which is positive if and only if $M > (4N_S)^{-1}$.

These conditions are easy to prove. In fact, note that $G > 0$ if and only if

$$\Delta := \mathcal{Q}(M,N_S) - \mathcal{C}(M,N_S) < 0. \tag{B3}$$

Thus, let us expand $\Delta = \Delta(M,N_S,N_B,1-\varepsilon)$ at the first order in ε. For a given $N_B > 0$, we have

$$\Delta = \tfrac{1}{2}[(MN_B\varepsilon)^{1/2} - M(N_B + N_S + 2N_BN_S)\varepsilon] + O(\varepsilon^{3/2}), \tag{B4}$$

which is negative if and only if

$$M > \frac{N_B}{(N_B + N_S + 2N_BN_S)^2\varepsilon} := \kappa(N_B). \tag{B5}$$

Notice that $\kappa(N_B)$ is maximum for

$$N_B^* = N_S(1+2N_S)^{-1}. \tag{B6}$$

Then, for every $N_B > 0$, we have $\Delta < 0$ if and only if

$$M > \kappa(N_B^*) = \frac{1}{4N_S(2N_S+1)\varepsilon}. \tag{B7}$$

Now, let us consider the particular case of $N_B = 0$. In this case, we have the first-order expansion

$$\Delta = (MN_S)^{1/2}[1 - 2(MN_S)^{1/2}]\varepsilon/4 + O(\varepsilon^2), \tag{B8}$$

or, equivalently, the second-order expansion of G given in Eq. (B2). It is clear that $\Delta < 0$, i.e., $G > 0$, when $M > 1/4N_S$. However, this condition is less restrictive than the one in Eq. (B7), which therefore can be extended to every $N_B \geqslant 0$.

2. High-energy asymptote ($r_0 = 0$)

Let us analyze the behavior of $M^{(N_S)}(r_0)$ for $N_S \geqslant 1$ and $r_0 = 0$. One can check that for $N_S \geqslant 1$, the greatest value of $M^{(N_S)}(0)$ occurs when $N_B = 0$. In this case, i.e., for $r_0 = N_B = 0$ and $r_1 = 1$, we have

$$\mathcal{Q}(M,N_S) = \frac{(1+N_S)^{-2M}}{2} \tag{B9}$$

and

$$\mathcal{C}(M,N_S) = \frac{1-\sqrt{1-e^{-MN_S}}}{2} \overset{M\gg 1}{\longrightarrow} \frac{e^{-MN_S}}{4} := \mathcal{C}^{\infty}. \tag{B10}$$

Let us consider the critical value $M^{(N_S)}(0)$ of M such that $G(M,N_S) = 0$, which is equivalent to $\mathcal{Q} = \mathcal{C}$. We also consider the value $\tilde{M}$ such that $\mathcal{Q} = \mathcal{C}^{\infty}$. We find that $M^{(N_S)}(0) \simeq \tilde{M}$ with very good approximation when $N_S \geqslant 1$ (see Fig. 7). Then, for every $N_S \geqslant 1$, we can set

$$M^{(N_S)}(0) \simeq \tilde{M} = (\ln 2)[2\ln(1+N_S) - N_S]^{-1}. \tag{B11}$$

The latter quantity becomes infinite for $2\ln(1+N_S) = N_S$, i.e., for $N_S \gtrsim 2.51$ photons.

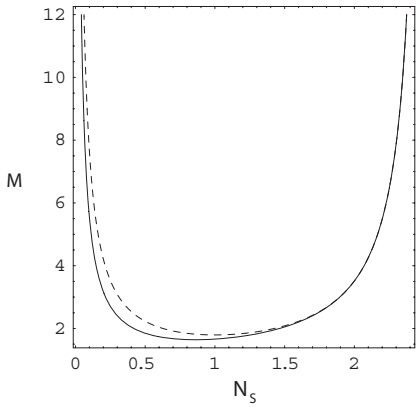

FIG. 7. Minimum number of signals M versus energy N_S. The solid curve represents $M^{(N_S)}(0)$ while the dashed curve represents $\tilde{M}$. Notice that the minimum number of signals is actually given by $\lceil M \rceil$, where $\lceil \cdots \rceil$ is the ceiling function.

[1] M. A. Nielsen and I. L. Chuang, *Quantum Computation and Quantum Information* (Cambridge University Press, Cambridge, 2000).

[2] S. L. Braunstein and A. K. Pati, *Quantum Information Theory with Continuous Variables*, (Kluwer Academic, Dordrecht, 2003).

[3] S. L. Braunstein and P. van Loock, Rev. Mod. Phys. **77**, 513 (2005).

[4] A. Ferraro, S. Olivares, and M. Paris, *Gaussian States in Quantum Information* (Biliopolis, Napoli, 2005).

[5] J. Eisert and M. B. Plenio, Int. J. Quant. Inf. **1**, 479 (2003).

[6] C. Weedbrook, S. Pirandola, R. García-Patrón, N. J. Cerf, T. C. Ralph, J. H. Shapiro, and S. Lloyd, Rev. Mod. Phys. **84**, 621 (2012).

[7] A. Furusawa, J. L. Sorensen, S. L. Braunstein, C. A. Fuchs, H. J. Kimble, and E. S. Polzik, Science **282**, 706 (1998).

[8] S. L. Braunstein and H. J. Kimble, Phys. Rev. Lett. **80**, 869 (1998).

[9] T. C. Ralph, Opt. Lett. **24**, 348 (1999).

[10] S. Pirandola, S. Mancini, D. Vitali, and P. Tombesi, Phys. Rev. A **68**, 062317 (2003).

[11] S. D. Bartlett and W. J. Munro, Phys. Rev. Lett. **90**, 117901 (2003).

[12] J. Sherson, H. Krauter, R. K. Olsson, B. Julsgaard, K. Hammerer, I. Cirac, and E. S. Polzik, Nature (London) **443**, 557 (2009).

[13] P. van Loock and S. L. Braunstein, Phys. Rev. Lett. **84**, 3482 (2000).

[14] S. Pirandola and S. Mancini, Laser Phys. **16**, 1418 (2006).

[15] S. Pirandola, S. Mancini, D. Vitali, and P. Tombesi, J. Mod. Opt. **51**, 901 (2004).

[16] S. Pirandola, Int. J. Quant. Inf. **3**, 239 (2005).

[17] S. Pirandola, S. Mancini, and D. Vitali, Phys. Rev. A **71**, 042326 (2005).

[18] P. van Loock and S. L. Braunstein, Phys. Rev. A **61**, 010302(R) (1999).

[19] N. Takei, H. Yonezawa, T. Aoki, and A. Furusawa, Phys. Rev. Lett. **94**, 220502 (2005).

[20] S. Pirandola, D. Vitali, P. Tombesi, and S. Lloyd, Phys. Rev. Lett. **97**, 150403 (2006).

[21] N. J. Cerf, M. Levy, and G. Van Assche, Phys. Rev. A **63**, 052311 (2001).
[22] F. Grosshans and P. Grangier, Phys. Rev. Lett. **88**, 057902 (2002).
[23] C. Weedbrook, A. M. Lance, W. P. Bowen, T. Symul, T. C. Ralph, and P. K. Lam, Phys. Rev. Lett. **93**, 170504 (2004).
[24] C. Weedbrook, A. M. Lance, W. P. Bowen, T. Symul, T. C. Ralph, and P. K. Lam, Phys. Rev. A **73**, 022316 (2006).
[25] S. Pirandola, S. L. Braunstein, and S. Lloyd, Phys. Rev. Lett. **101**, 200504 (2008).
[26] C. Weedbrook, S. Pirandola, S. Lloyd, and T. C. Ralph, Phys. Rev. Lett. **105**, 110501 (2010).
[27] S. Pirandola, S. Mancini, S. Lloyd, and S. L. Braunstein, Nat. Phys. **4**, 726 (2008).
[28] I. Devetak, IEEE Trans. Inf. Theory **5**, 44 (2005).
[29] S. Pirandola, R. García-Patrón, S. L. Braunstein, and S. Lloyd, Phys. Rev. Lett. **102**, 050503 (2009).
[30] V. Scarani, H. Bechmann-Pasquinucci, N. J. Cerf, M. Dusek, N. Lutkenhaus, and M. Peev, Rev. Mod. Phys. **81**, 1301 (2009).
[31] S. Lloyd and S. L. Braunstein, Phys. Rev. Lett. **82**, 1784 (1999).
[32] D. Gottesman, A. Kitaev, and J. Preskill, Phys. Rev. A **64**, 012310 (2001).
[33] B. C. Travaglione and G. J. Milburn, Phys. Rev. A **66**, 052322 (2002).
[34] S. Pirandola, S. Mancini, D. Vitali, and P. Tombesi, Europhys. Lett. **68**, 323 (2004).
[35] S. Glancy and E. Knill, Phys. Rev. A **73**, 012325 (2006).
[36] S. Pirandola, S. Mancini, D. Vitali, and P. Tombesi, J. Phys. B **39**, 997 (2006).
[37] S. Pirandola, S. Mancini, D. Vitali, and P. Tombesi, Eur. Phys. J. D **37**, 283 (2006).
[38] A. P. Lund, T. C. Ralph, and H. L. Haselgrove, Phys. Rev. Lett. **100**, 030503 (2008).
[39] S. Sefi and P. van Loock, Phys. Rev. Lett. **107**, 170501 (2011).
[40] R. Raussendorf and H. J. Briegel, Phys. Rev. Lett. **86**, 5188 (2001).
[41] N. C. Menicucci, P. van Loock, M. Gu, C. Weedbrook, T. C. Ralph, and M. A. Nielsen, Phys. Rev. Lett. **97**, 110501 (2006).
[42] J. Zhang and S. L. Braunstein, Phys. Rev. A **73**, 032318 (2006).
[43] S. T. Flammia, N. C. Menicucci, and O. Pfister, J. Phys. B **42**, 114009 (2009).
[44] N. C. Menicucci, X. Ma, and T. C. Ralph, Phys. Rev. Lett. **104**, 250503 (2010).
[45] L. Aolita, A. J. Roncaglia, A. Ferraro, and A. Acín, Phys. Rev. Lett. **106**, 090501 (2011).
[46] A. Einstein, B. Podolsky, and N. Rosen, Phys. Rev. **47**, 777 (1935).
[47] For two bosonic modes, A and B, with quadratures $\hat{q}_A$, $\hat{p}_A$, $\hat{q}_B$, and $\hat{p}_B$, one can define the two operators $\hat{q}_- := (\hat{q}_A - \hat{q}_B)/\sqrt{2}$ (relative position) and $\hat{p}_+ := (\hat{p}_A + \hat{p}_B)/\sqrt{2}$ (total momentum). Then the system has EPR correlations (in these operators) if $V(\hat{q}_-) + V(\hat{p}_+) < 2\nu_0$, where $V(\cdot)$ is the variance and ν_0 is the standard quantum limit ($\nu_0 = 1$ in this paper.) A bosonic system with EPR correlations is entangled, but the contrary is not necessarily true. The EPR correlations represent the most typical kind of continuous-variable entanglement and are usually generated by parametric down conversion.
[48] E. C. G. Sudarshan, Phys. Rev. Lett. **10**, 277 (1963).
[49] R. J. Glauber, Phys. Rev. **131**, 2766 (1963).
[50] S.-H. Tan, B. I. Erkmen, V. Giovannetti, S. Guha, S. Lloyd, L. Maccone, S. Pirandola, and J. H. Shapiro, Phys. Rev. Lett. **101**, 253601 (2008).
[51] S. Lloyd, Science **321**, 1463 (2008).
[52] J. H. Shapiro and S. Lloyd, New J. Phys. **11**, 063045 (2009).
[53] S. Guha and B. I. Erkmen, Phys. Rev. A **80**, 052310 (2009).
[54] A. R. Usha Devi and A. K. Rajagopal, Phys. Rev. A **79**, 062320 (2009).
[55] H. P. Yuen and R. Nair, Phys. Rev. A **80**, 023816 (2009).
[56] S. Pirandola, Phys. Rev. Lett. **106**, 090504 (2011).
[57] R. Nair, Phys. Rev. A **84**, 032312 (2011).
[58] O. Hirota, arXiv:1108.4163.
[59] A. Bisio, M. Dall'Arno, and G. M. D'Ariano, Phys. Rev. A **84**, 012310 (2011).
[60] M. Dall'Arno, A. Bisio, G. M. D'Ariano, M. Miková, M. Ježek, and M. Dušek, Phys. Rev. A **85**, 012308 (2012).
[61] S. Pirandola, C. Lupo, V. Giovannetti, S. Mancini, and S. L. Braunstein, New J. Phys. **13**, 113012 (2011).
[62] S. Guha, Z. Dutton, R. Nair, J. Shapiro, and B. Yen, *Information Capacity of Quantum Reading*, in Laser Science, OSA Technical Digest, Paper LTuF2 (Optical Society of America, 2011).
[63] M. M. Wilde, S. Guha, S.-H. Tan, and S. Lloyd, arXiv:1202.0518.
[64] T. M. Cover and J. A. Thomas, *Elements of Information Theory* (Wiley, Hoboken, NJ, 2006).
[65] C. W. Helstrom, *Quantum Detection and Estimation Theory* (Academic Press, New York, 1976).
[66] C. A. Fuchs and J. V. de Graaf, IEEE Trans. Inf. Theory **45**, 1216 (1999).
[67] C. Fuchs, Ph.D. thesis, University of New Mexico, 1995.
[68] K. M. R. Audenaert, J. Calsamiglia, R. Munoz-Tapia, E. Bagan, L. Masanes, A. Acin, and F. Verstraete, Phys. Rev. Lett. **98**, 160501 (2007).
[69] J. Calsamiglia, R. Munoz-Tapia, L. Masanes, A. Acin, and E. Bagan, Phys. Rev. A **77**, 032311 (2008).
[70] M. Nussbaum and A. Szkoła, Ann. Stat. **37**, 1040 (2009).
[71] K. M. R. Audenaert, M. Nussbaum, A. Szkoła, and F. Verstraete, Commun. Math. Phys. **279**, 251 (2008).
[72] S. Pirandola and S. Lloyd, Phys. Rev. A **78**, 012331 (2008).
[73] S. Pirandola, A. Serafini, and S. Lloyd, Phys. Rev. A **79**, 052327 (2009).
[74] R. Simon, N. Mukunda, and B. Dutta, Phys. Rev. A **49**, 1567 (1994).
[75] J. Williamson, Am. J. Math. **58**, 141 (1936).
[76] G. Spedalieri, C. Weedbrook, and S. Pirandola, arXiv:1204.2473.
[77] H. Nha and H. J. Carmichael, Phys. Rev. A **71**, 032336 (2005).
[78] S. Olivares, M. G. A. Paris, and U. L. Andersen, Phys. Rev. A **73**, 062330 (2006).
[79] H. Scutaru, J. Phys. A **31**, 3659 (1998).